# Simple method for the characterization of intense Laguerre-Gauss vector vortex beams

E. Allahyari,[1,2] J. JJ Nivas,[1,2] F. Cardano,[1] R. Bruzzese,[1,2] R. Fittipaldi,[3] L. Marrucci,[1] D. Paparo,[4] A. Rubano,[1] A. Vecchione,[3] and S. Amoruso[1,2]

[1]Dipartimento di Fisica, Università di Napoli Federico II, Complesso Universitario di Monte S. Angelo, Via Cintia, I-80126 Napoli, Italy
[2]CNR-SPIN, UOS Napoli, Complesso Universitario di Monte S. Angelo, Via Cintia, I-80126 Napoli, Italy
[3]CNR-SPIN, UOS Salerno, Via Giovanni Paolo II 132, I-84084 Fisciano, Italy.
[4]National Research Council, Institute of Applied Science & Intelligent Systems (ISASI) 'E. Caianiello', Via Campi Flegrei 34, 80078 Pozzuoli (NA), Italy

We report on a method for the characterization of intense, structured optical fields through the analysis of the size and surface structures formed inside the annular ablation crater created on the target surface. In particular, we apply the technique to laser ablation of crystalline silicon induced by femtosecond vector vortex beams. We show that a rapid direct estimate of the beam waist parameter is obtained through a measure of the crater radii. The variation of the internal and external radii of the annular crater as a function of the laser pulse energy, at fixed number of pulses provides another way to evaluate the beam spot size through numerical fitting of the obtained experimental data points. A reliable estimate of the spot size is of paramount importance to investigate pulsed laser-induced effects on the target material. Our experimental findings offer a facile way to characterize focused, high intensity complex optical vector beams which are more and more applied in laser-matter interaction experiments.

Structured light beams with non-Gaussian, customized intensity profiles and spatially variant state of polarization (SoP) are gaining attention as a novel prospect in many fields of optical science and technology[1–4]. In this context, optical vortices exhibiting a spiral phase structure and an annular spatial intensity distribution around the beam axis and transporting orbital angular momentum (OAM) are being widely used in a number of applications, e.g., optical tweezers, phase contrast microscopy, stimulated emission depletion microscopy and lithography, micro-manipulation and micro-machines, photo-polymerization, etc..[1–3] Similarly, vector-vortex beams, obtained when superimposing left and right circularly polarized beams (or any pair of orthogonal polarization states) carrying opposite values of OAM, and characterized by topologically non-trivial polarization pattern, are exploited in various applications. Recently, the progressive development of efficient beam converters generating powerful, pulsed optical vortex (OV) and vector-vortex (VV) beams is offering the possibility of experimenting with such complex light beams and observing new experimental aspects in other emerging applications, like direct laser processing and surface structuring. For example, chiral micro-needles on various metals, silicon and azo-polymer are created by OV beams with nanosecond pulse duration.[5–7] Femtosecond (fs) optical vortices are exploited in the micro-fabrication of various structures like cavities in glasses,[8] single-layer graphene disks,[9] polymer tubes,[10,11] silicon conical structures,[12] etc.. Moreover, VV beams with variable SoP and intensity have been shown to form interesting surface patterns and biomimetic structures on the material surface, which are not achievable by the standard beams with a Gaussian intensity profile.[13–16]

Nowadays, the use of complex light beams in surface micro-processing is emerging as an attractive prospect and a promising approach to fabricate functional elements with complex surface structures. Laser-induced modifications of the material surface (e.g. phase transformation, melting, ablation, structure features, etc.) can strictly depend on the local state of the beam (e.g., fluence and polarization), therefore a careful characterization of the beam properties is paramount to gain reliable knowledge on the

mechanisms involved in several transformation processes. For intense Gaussian laser beams, Liu introduced a simple technique to estimate the beam spot size,[17] based on the analysis of the variation of the area modified by the laser irradiation vs laser energy. Such an approach is generally exploited in experiments with intense beams and is also corroborated by theoretical results in the case of fs laser ablation.[18] Recently, a similar approach was applied to ablation of Au films irradiated by OV beams generated by coupling a spiral phase plate to an axicon,[19] and to laser processing of silicon with VV beams produced by a q-plate with a topological charge $q = 1/2$.[20]

Here we illustrate an effective method for characterizing the VV beam properties through analysis of the annular craters produced in fs laser ablation of silicon. In particular, we show that a direct estimate of the beam spot size can be easily obtained by measuring internal and external radii of the annular crater, meanwhile the variation of the radii as a function of the laser pulse energy provides a more accurate way to evaluate the beam spot size through a best fit procedure. Our approach for the detection of the beam waist parameter applies to the specific case of VV beams whose radial profile is that of Laguerre-Gauss (LG) beams, in the lowest radial mode with $p=0$. Let us note that, although we refer here to the case of VV beam, this method can be applied also to uniformly polarized beams, i.e. scalar fields, whose spatial structure is that of LG beams carrying OAM. A more complete characterization of the VV beams is eventually accomplished by visualization of the laser induce periodic surface structures that has been shown earlier to offer a general method to reconstruct the local orientation of the polarization state.[13,14,16,20,21] Here, we confirm the good agreement between the beam SoP and the surface structures also for more complex VV beams with larger OAM values. In metals and semiconductors, at a fixed number of irradiating pulses, linearly polarized light leads to sub-wavelength ripples oriented normal to the electric field direction above the ablation fluence threshold. In the case of dielectrics, the laser induced surface structures follow the local direction of the laser polarization.[21,22] In the case of semiconductors, as silicon, also supra-wavelength grooves parallel to laser polarization form at larger fluence values, while coarser stripes and columnar structures are produced at still higher fluence,[15,22–24] which may allow a

qualitative reconstruction of the fluence spatial distribution.[24] In the present study, silicon is selected because it is the most basic and studied semiconductor material, on which well-defined surface structures forms under fs laser irradiation.[22–26] However, the method can be applied to annular VV beams irradiation of other materials at different number of pulses, according to their ablation threshold, and even in tight focusing conditions unless the very specific case of a strong longitudinal field component at the focal plane,[3,8] which can strongly change the fluence spatial profile.

A fs Ti:Sa system is used as laser source providing linearly polarized pulses of ≈ 35 fs duration and 800 nm wavelength, with a Gaussian beam spatial profile, at 100 Hz repetition rate. VV beams are generated by shining different q-plates ($q$ = 1/2, 1, 3/2, 2, 5/2)[27,28] with these laser beams, thus obtaining VV beams with an annular spatial profile, where left and right circular polarization components carry OAM with values $\ell = \pm 2q$ ($\ell$ = 1, 2, 3, 4, 5), respectively.[29] Q-plates are essentially made of two glass plates separated by a thin layer of liquid crystals, whose optic axes have been arranged in a singular pattern with topological charge $q$, the latter being an integer or half-integer number.[27,28] Using cylindrical coordinates with the $z$ being the propagation axis, the spatial distribution of the optical field can be expressed as:

$$\psi_{VV}^{(l)} \propto f_\ell(r,z)(\boldsymbol{e_l}\, e^{i\,\ell\,\varphi} + \boldsymbol{e_r}\, e^{-i\,\ell\,\varphi}) \tag{1}$$

where $\boldsymbol{e_l}$ and $\boldsymbol{e_r}$ are the unit vectors associated with the left and right circular polarization states and $\varphi$ the azimuthal angle. The temporal dependence of the field, inherited from the input laser light generated by the Ti:Sa system, is not shown here. In this setup indeed it can be treated as a global term not affecting the spatial and polarization structure of the field. The normalized function $f_\ell(r,z)$, that describes the radial distribution of the field, is identical for the two modes carrying opposite value of OAM $\pm\ell$. In general, at the exit of the q-plate, the radial profile is that of Hyper-Geometric Gaussian modes.[30,31] However, by filtering the beam with a circular aperture, we observe that beam profile is well approximated by Laguerre-Gauss mode, as discussed below (see Figs. 1(a) and (c)).

The beam is focused with a lens with a nominal focal length of 75 mm on the surface of a (100) silicon

4

target, in air. The target is mounted on a XY-translation stage located perpendicular to the laser beam direction. The beam energy $E$ is varied by tuning the energy of the input Gaussian beam with a combination of a half wave plate and a polarizer, while the desired number of laser pulses ($N$) applied to the same spot on the target is selected by means of an electromechanical shutter. The morphology of the ablation crater surface is analyzed by scanning electron microscopy (SEM).

Fig. 1(a) reports the annular spatial intensity distribution of the beam generated by our system with a q-plate with $q=1/2$ before the focusing lens, which exemplifies the typical donut shape of VV beams with a central region of zero intensity, due to an undefined phase on the beam axis. As an example, Fig. 1(b) reports an annular crater ($N = 200$, $E \approx 40$ µJ, $q=1$) whose shape addresses the good azimuthal symmetry of the fluence spatial distribution of the VV beams. Fig. 1(c) shows examples of cross sectional profiles of the beam generated by the $q$-plate for three different values of $q$, namely $q = 1/2$, 1, 5/2, registered by a CCD positioned after the aperture. In Fig. 1(c), the symbols represent experimental data points and the error bar on each cross sectional profile illustrates the corresponding variability thus addressing the good axial symmetry of the VV beams. The error bars were obtained by estimating the standard deviation on several different cross sectional profiles registered at various azimuthal angles. In Fig. 1(c), the solid curves are approximate theoretical profiles of the fluence spatial distribution $F_\ell(r)$ in terms of the Laguerre-Gauss modes subclass $LG_{0,\ell}$,[3] as:

$$\frac{F_\ell(r)}{F_{\ell,peak}} = c_\ell \left(\frac{\sqrt{2}r}{w_0}\right)^{2\ell} e^{-\frac{2r^2}{w_0^2}} \tag{2}$$

where $c_\ell = e^{+\ell}/\ell^\ell$ is a normalization factor and $w_0$ is the beam waist. The peak value of the fluence profile is located on a circle of radius $r_p$, given by:

$$r_p = \sqrt{\frac{\ell}{2}} w_0 \tag{3}$$

and the corresponding value of the peak fluence is

$$F_{\ell,peak} = F_\ell(r_p) = \frac{2e^{-\ell}\ell^\ell}{\ell!} \frac{E}{\pi w_0^2} \tag{4}$$

As shown in Fig. 1(c), Eq. (2) fits the experimental data rather well with a value of the beam waist after the q-plate $w_{0,in}=(0.40\pm0.02)$ mm.
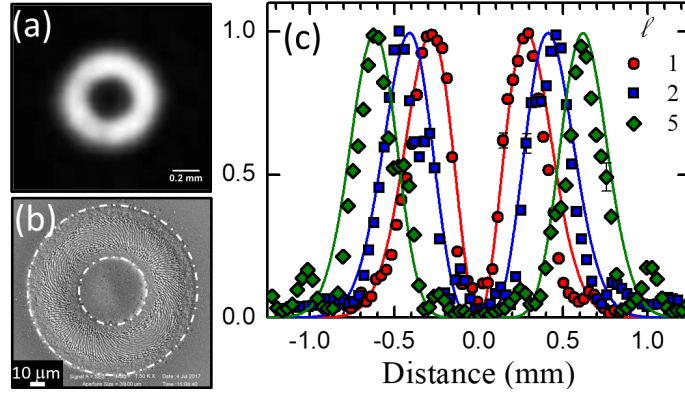


FIG. 1. (a) Annular spatial intensity distribution of the VV beam generated by a q-plate with $q=1/2$. (b) Example of an annular crater ($N=200$, $E\approx40$ μJ, $q=1$) produced by a VV beam. The internal and external circles (dashed lines) delimit the ablated area. (c) Normalized cross sectional profiles of the intensity for three different values of the OAM, $\ell$: symbols - experimental data; solid curves – fluence profiles according to Eq. (2) with $w_0$=0.40 mm. The error bar on each cross sectional profile illustrates its typical variability.

| $\ell$ | 1 | 2 | 3 | 4 | 5 | |
|---|---|---|---|---|---|---|
| $w_0$ | 44±3 | 42±1 | 44±1 | 47±4 | 43±2 | *Eq. (6)* |
| | 43±3 | 41±3 | 44±3 | 48±5 | 43±3 | *Eq. (7)* |

Table I: values of the beam spot size $w_0$ (in μm) as obtained by using Eq. (6) and numerical fitting to Eq.(7) for various VV beams with different OAM, $\ell$.

VV beams generated by the q-plate also have a spatially variable polarization depending on the OAM value, as described in Eq. (1).[29] As an example, Fig. 2(a) reports the expected pattern of the SoP for a VV beam with $\ell=4$ in which the arrows indicate the direction of the electric field. Fig. 2(b) shows the SEM image of the crater produced by irradiating the target with $N=100$ laser pulses, at an energy $E\approx80$ μJ. The surface of the annular crater presents surface structures oriented according to the local laser polarization, as can be recognized in the zoomed views shown in Figs. 3(c) and 3(d). In Fig. 3(c), one can appreciate the rather direct correspondence between the grooves orientation and the SoP pattern of Fig. 2(a). Moreover, at the inner and external sides of the annular grooved region, two rings are present with

ripples directed along the normal to the local laser polarization direction, as exemplified in Fig. 2(d). The spatial distribution of these structures qualitatively follows the variation of the local laser fluence, with grooves covering the higher fluence region and ripples localized in the less intense part of the beam. This, in turn, confirms the close correspondence between the beam SoP and the surface structures also for the more complex VV beams with larger OAM values.
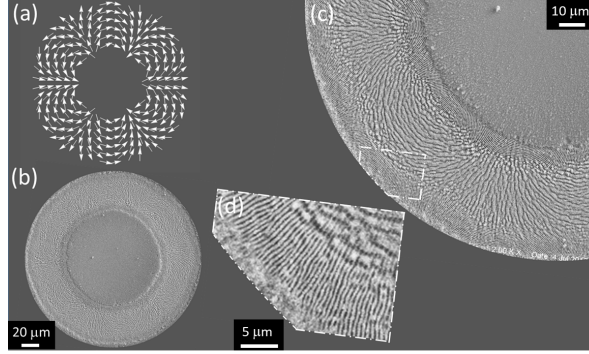


FIG. 2. (a) Typical spatial pattern of the SoP for a beam with $\ell = 4$; the arrows indicate the local direction of the electric field. (b) SEM image of the crater produced by irradiating the target with $N = 100$ laser pulses, at an energy $E \approx 80$ μJ. Panels (c) and (d) report zoomed views of the surface structures registered at higher magnification.

We turn now to the analysis of the crater to gain an estimate of the beam spot size in the focal plane. We assume that the field intensity distribution in the focal plane is also described by LG modes of Eq. (2), characterized by a waist parameter equal to $w_{0f}$. From propagation optics,[32] one can estimate an expected value of the beam waist at the focal plane $w_{of} = \frac{\lambda f}{\pi w_{0,in}} \left( 1 + \frac{f^2}{w_{0,in}^2} \right)^{-1/2}$ that yields a value of $(47 \pm 2)$ μm.

The annular ablation crater is limited by the internal, $r_{in}$, and external, $r_{ex}$, radii, at which the pulse fluence equals the ablation threshold fluence, therefore $F_\ell(r_{in}) = F_\ell(r_{ex})$. From Eqs. (2), this yields:

$$\left( \frac{r_{in}}{w_0} \right)^{2\ell} e^{-\frac{2r_{in}^2}{w_0^2}} = \left( \frac{r_{ex}}{w_0} \right)^{2\ell} e^{-\frac{2r_{ex}^2}{w_0^2}} \tag{5}$$

Solving for $w_0$ one gets:

$$w_0 = \sqrt{\frac{(r_{ex}^2 - r_{in}^2)}{\ell \, ln\left(\frac{r_{ex}}{r_{in}}\right)}} \tag{6}$$

Eq. (6) provides a direct and simple way to evaluate the VV beam waist $w_0$ from the measurement of a couple of values ($r_{in}$, $r_{ex}$). This was applied to the craters produced by VV beams at various values of the charge $l$ and the estimates are summarized in Table I. In our procedure, we carry out direct measurements of the internal and external crater circles (see Fig. 1(b), e.g.), which take into account uncertainties due to both the actual beam spatial profile and the variability of circle recognition obtained in repeated measurements by different individuals in our team. From double-circles measurements, the mean and standard deviation of the internal and external radii ($r_{in}$, $r_{ex}$) are obtained for different values of the pulse energy $E$ at each $\ell$ and the corresponding $w_0$ is estimated. Within the limited statistics (in some cases only few values were used, e.g. for $\ell = 4$), the data show a fairly good consistency and the variation and uncertainties are likely due to the specific $q$-plate features and to laser pulse energy fluctuations. Moreover, the estimated values show a good consistency with the expected estimate of $w_{of}$ above reported.
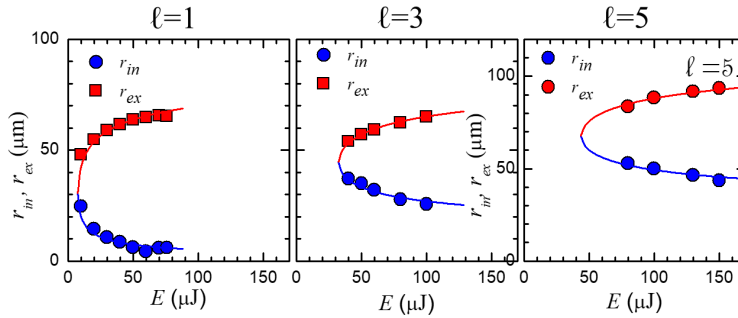


FIG. 3. Examples of the variation of the internal $r_{in}$ (blue circles) and $r_{ex}$ external (red squares) radii as a function of the VV beam energy $E$ for three values of $\ell$, reported on the top of each panel. The number of laser pulses is $N = 100$ for $\ell = 1$ and N = 200 for $\ell = 3$ and $\ell = 5$, respectively.

We turn now to the dependence of the internal and external radii on the pulse energy. As an example, Fig. 3 reports the variation of $r_{in}$ and $r_{ex}$ on $E$ for three values of the OAM, $\ell$. One can observe a gradual decrease of the ablated annular region, whose width ($r_{ex} - r_{in}$) diminishes as the energy $E$ reduces. The

8

observed dependence can be described as a solution of the equation:

$$F_\ell(r) = F_{th} \tag{7}$$

$F_{th}$ being the value of the ablation threshold at the selected experimental conditions, i.e. the minimum

pulse fluence required to induce ablation at the given number of pulses, $N$.[18,26]

An analytical solution for Eq. (7) does not exist, however best fits to the experimental data can be obtained

through a numerical least-square minimization procedure. By using the beam waist $w_0$ and the threshold

fluence $F_{th}$ as fitting parameters, the curves reported as solid lines in Fig. 3 were obtained. The obtained

values of $w_0$ are reported in Table I and result in good agreement with the previous estimates given by

Eq. (6). The curves describe fairly well the experimental data with two branches departing from a radius

$r_p$, at which the ablated region degenerates into a limiting circumference (i.e., $r_{ex} = r_{in} = r_p$), and a value

of $E_{th}$, below which no surface ablation occurs at the selected number of pulses, $N$. The variation of $r_p$ as

a function of the OAM is shown in Fig. 4. The solid line is a fitting curve to the dependence $r_p = \frac{w_0}{\sqrt{2}}\ell^\alpha$

yielding $w_0 = (43\pm3)$ µm and $\alpha = (0.53\pm0.05)$, in fairly good agreement with Eq. (3). The value of $E_{th}$ is

consistent with the ablation threshold $F_{th}$. The obtained values of $F_{th}$ are $(0.10\pm0.02)$ J/cm$^2$ for the silicon

sample irradiated by $N = 100$ VV laser pulses with $\ell = 1$ and $(0.21\pm0.05)$ J/cm$^2$ for the sample irradiated

by $N=200$ laser pulses with $\ell = (2\div5)$. The ablation threshold depends upon the material properties, the

pulse characteristics and the number of applied pulses, $N$.[26,33] In particular, $F_{th}$ generally decreases at

larger number of pulses. The different values of $F_{th}$ registered in the present case are due to the different

characteristics of the sample target used in the experiments carried out with $\ell = 1$ and for $\ell = (2\div5)$ VV

beams, respectively. In fact, in the latter case intrinsic Si (100) samples (resistivity $> 200$ $\Omega$cm) were used

as targets, while in the former case a p-doped Si (100) plate (resistivity $15\div25$ $\Omega$cm) was exploited. The

value of the ablation threshold for the intrinsic silicon is in agreement with recent values reported for

undoped Si ablated by 800 nm, $\approx 110$ fs laser pulses.[33] Moreover, the reduction of the ablation threshold

observed for the doped Si sample is likely due to the increase of free carrier concentration, as
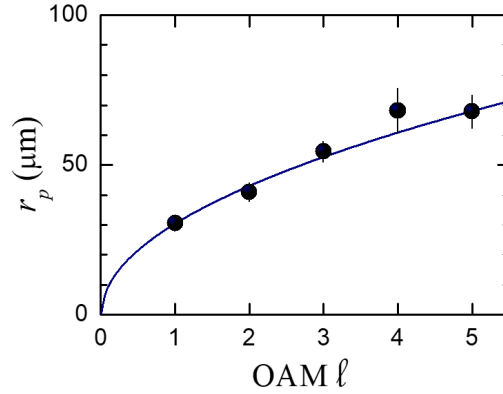
demonstrated in recent reports.[33,34]



FIG. 4. Variation of the peak radius, $r_p$, as a function of the value of the index $\ell$. The line is a fitting curve to the relation $r_p = \frac{w_0}{\sqrt{2}} \ell^\alpha$ yielding $w_0 = (43\pm3)$ μm and $\alpha = (0.53\pm0.05)$ in fairly good agreement with Eq. (3).

Finally, we would like to stress that a reliable measure of the beam waist is paramount in order to address the mechanisms involved in laser-induced modifications of a material. For example, we estimated the fluence level for which the transition from a rippled to a grooved pattern occurs after $N = 100$ laser pulses for the various OV beams considered above. We observe that for $\ell = 1$ such a transition occurs at $\approx 0.24$ J/cm$^2$, while for $\ell=(2\div5)$ it takes place at $\approx 0.5$ J/cm$^2$. Such observation suggests that the level of doping of the silicon target also influences the grooves formation process, besides determining the ablation threshold.

In conclusion, we illustrated a simple and direct experimental method based on the analysis of laser ablation spots that allows ascertaining fs VV beam properties. Our approach demonstrates a reliable characterization of intense fs VV beams in weak focusing conditions, which are more and more exploited in fs laser micro-processing applications. In particular, we have discussed various ways to gather an estimate of the beam spot size that eventually defines the spatial profile of the laser fluence. Furthermore, our findings confirms that the orientation of the laser-induced surface structures provides a direct clue on the local polarization of the beam. The proposed approach can likely be extended to other materials or to VV beams with still higher OAM values in their polarization components. Finally, an appropriate

10

selection of the target material and type of modification can allow a reliable and precise characterization of VV beams at other laser wavelengths.

[1] J. Secor, R. Alfano, and S. Ashrafi, *Complex Light* (IOP Publishing, 2016).

[2] J.P. Torres and L. Torner, *Twisted Photons : Applications of Light with Orbital Angular Momentum* (Wiley-VCH Verlag, 2011).

[3] Q. Zhan, Adv. Opt. Photonics **1**, 1 (2009).

[4] H. Rubinsztein-Dunlop, A. Forbes, M. V Berry, M.R. Dennis, D.L. Andrews, M. Mansuripur, C. Denz, C. Alpmann, P. Banzer, T. Bauer, E. Karimi, L. Marrucci, M. Padgett, M. Ritsch-Marte, N.M. Litchinitser, N.P. Bigelow, C. Rosales-Guzmán, A. Belmonte, J.P. Torres, T.W. Neely, M. Baker, R. Gordon, A.B. Stilgoe, J. Romero, A.G. White, R. Fickler, A.E. Willner, G. Xie, B. McMorran, and A.M. Weiner, J. Opt. **19**, 13001 (2017).

[5] T. Omatsu, K. Miyamoto, and R. Morita, in *Vor. Dyn. Opt. Vor.* (InTech, 2017).

[6] S. Syubaev, A. Zhizhchenko, A. Kuchmizhak, A. Porfirev, E. Pustovalov, O. Vitrik, Y. Kulchin, S. Khonina, and S. Kudryashov, Opt. Express **25**, 10214 (2017).

[7] D. Barada, G. Juman, I. Yoshida, K. Miyamoto, S. Kawata, S. Ohno, and T. Omatsu, Appl. Phys. Lett. **108**, 51108 (2016).

[8] C. Hnatovsky, V.G. Shvedov, W. Krolikowski, and A. V. Rode, Opt. Lett. **35**, 3417 (2010).

[9] B. Wetzel, C. Xie, P.-A. Lacourt, J.M. Dudley, and F. Courvoisier, Appl. Phys. Lett. **103**, 241111 (2013).

[10] E. Stankevicius, T. Gertus, M. Rutkauskas, M. Gedvilas, G. Raciukaitis, R. Gadonas, V.

Smilgevicius, and M. Malinauskas, J. Micromechanics Microengineering **22**, 65022 (2012).

[11] L. Yang, D. Qian, C. Xin, Z. Hu, S. Ji, D. Wu, Y. Hu, J. Li, W. Huang, and J. Chu, Appl. Phys. Lett. **110**, 221103 (2017).

[12] M.G. Rahimian, F. Bouchard, H. Al-Khazraji, E. Karimi, P.B. Corkum, and V.R. Bhardwaj, APL Photonics **2**, 86104 (2017).

[13] J. JJ Nivas, S. He, A. Rubano, A. Vecchione, D. Paparo, L. Marrucci, R. Bruzzese, and S. Amoruso, Sci. Rep. **5**, 17929 (2015).

[14] E. Skoulas, A. Manousaki, C. Fotakis, and E. Stratakis, Sci. Rep. **7**, 45114 (2017).

[15] J. JJ Nivas, Z. Song, R. Fittipaldi, A. Vecchione, R. Bruzzese, and S. Amoruso, Appl. Surf. Sci. **417**, 149 (2017).

[16] K.K. Anoop, A. Rubano, R. Fittipaldi, X. Wang, D. Paparo, A. Vecchione, L. Marrucci, R. Bruzzese, and S. Amoruso, Appl. Phys. Lett. **104**, (2014).

[17] J.M. Liu, Opt. Lett. **7**, 196 (1982).

[18] D. Bouilly, D. Perez, and L.J. Lewis, Phys. Rev. B **76**, 184119 (2007).

[19] R. Sahin, T. Ersoy, and S. Akturk, Appl. Phys. A **118**, 125 (2015).

[20] J. JJ Nivas, H.E. Shutong, K.K. Anoop, A. Rubano, R. Fittipaldi, A. Vecchione, D. Paparo, L. Marrucci, R. Bruzzese, and S. Amoruso, Opt. Lett. **40**, (2015).

[21] A. Papadopoulos, E. Skoulas, G.D. Tsibidis, and E. Stratakis, Appl. Phys. A **124**, 146 (2018).

[22] T.-H. Her, in *Compr. Nanosci. Technol.*, edited by D. Andrews, G. Scholes, and G. Wiederrecht (Elsevier, 2011), pp. 277–314.

[23] A.Y. Vorobyev and C. Guo, Laser Photonics Rev. **7**, 385 (2013).

[24] S. He, J. JJ Nivas, A. Vecchione, M. Hu, and S. Amoruso, Opt. Express **24**, 3238 (2016).

[25] J. JJ Nivas, S. He, Z. Song, A. Rubano, A. Vecchione, D. Paparo, L. Marrucci, R. Bruzzese, and S. Amoruso, Appl. Surf. Sci. **418**, 565 (2017).

[26] J. Bonse, H. Sturm, D. Schmidt, and W. Kautek, Appl. Phys. A Mater. Sci. Process. **71**, 657 (2000).

[27] L. Marrucci, C. Manzo, and D. Paparo, Phys. Rev. Lett. **96**, 163905 (2006).

[28] L. Marrucci, E. Karimi, S. Slussarenko, B. Piccirillo, E. Santamato, E. Nagali, and F. Sciarrino, J. Opt. **13**, 64001 (2011).

[29] F. Cardano, E. Karimi, S. Slussarenko, L. Marrucci, C. de Lisio, and E. Santamato, Appl. Opt. **51**, C1 (2012).

[30] E. Karimi, B. Piccirillo, L. Marrucci, and E. Santamato, Opt. Lett. **34**, 1225 (2009).

[31] G. Vallone, A. Sponselli, V. D'Ambrosio, L. Marrucci, F. Sciarrino, and P. Villoresi, Opt. Express **24**, 16390 (2016).

[32] A. Yariv, *Quantum Electronics*, 3rd Ed. (Wiley, New York, 1989).

[33] R.N. Oosterbeek, C. Corazza, S. Ashforth, and M.C. Simpson, Appl. Phys. A **122**, 449 (2016).

[34] J. Fang, L. Jiang, Q. Cao, K. Zhang, Y. Yuan, and Y. Lu, Appl. Opt. **53**, 3897 (2014).